WEES-2020 Special Issue

J. Indian Chem. Soc.,
Vol. 97, No. 10b, October 2020, pp. 1959-1966

Nusselt number and flow distribution analysis over the roughened surface in a rectangular channel of a solar air heater

Amit Kumar* and Apurba Layek

National Institute of Technology Durgapur, Durgapur-713 209, West Bengal, India

E-mail: amit4310@rediffmail.com

Manuscript received online 16 June 2020, revised and accepted 02 September 2020

This paper provides the experimental investigation on the latest development of the optical method primarily based on liquid crystals thermography (LCT) method, which is understood to be a vital tool to obtain surface temperature distribution and assessment of heat transfer coefficients of a rectangular channel using artificial rib roughness. The LCT approach makes use of thermo chromic liquid crystals, an organic material applied at heated surface in an effort to get the color response, which is snapped by a CCD camera on the premise of temperature modifications. The acquired color sample is digitized and decoded into its HSI (hue, saturation, and intensity) value by the $R_rG_gB_b$ (red, green, blue) response. The effect of roughness parameters taken into consideration encompasses relative roughness pitch (P_i/e) values of 6–12, attack angle (α) of 30°–75° and relative roughness width (W/*w*) of 3–6 on the improvement of heat transfer are investigated over by varying Reynolds number (Re) levels from 13500–20500. The objective is to get the Nusselt number variety distribution over the artificially roughened surface with uniform heat flux conditions. It is noted that relative roughness pitch (P_i/e) of 8, W/*w* of 5 at an attack angle (α) of 60° suggests its most beneficial value of heat transfer as compared to smooth absorber surface.

Keywords: Solar air heater, Nusselt number, winglet ribs, liquid cristal thermography.

Introduction

The augmentation in heat transfer rate of solar air heater system can be achieved by placing vortex generators of different shapes i.e. circular wire ribs, fins, winglets, obstacle, and perforated blocks between flowing fluid and the heated absorber plate. Generally, the vortex generators have been fabricated to cause interruption as well as the uniform mixing of the flowing fluid in the boundary layer. Now-a-days liquid crystal thermography technique were widely used to formulate the qualitative information regarding temperature distribution using thermo chromic liquid crystals sheet pasted on the heated surface. It is an optical technique to visualize the effect of temperature distribution through a color response on the heated surface leading to get convective heat transfer coefficient distribution. In the last decade, the number of research work has been made by approaching towards Liquid Crystal Thermography (LCT) technique for various heat transfer applications. Chan *et al.*[1] did the investigation using LCT approach on oblique/curved surface in order to get the heat transfer distribution. Copper *et al.*[2] implemented a problem-based study using LCT technique for augmentation in heat transfer. Tariq *et al.*[3] did the LCT based investigation on ribs with a continuous slit which is used to evaluate the Nusselt number distribution. Analysis has been done on different shape vortex generators by Liou *et al.*[4], Tanda[5] and Diego Cavallero[6] evaluated the roughness effect on heat transfer as well as pressure penalty in a rectangular duct with roughened rib. Andallib Tariq *et al.*[7] obtained detailed heat transfer and temperature distribution from flat and roughened surface by using LCT technique. Layek *et al.*[8] presented an experimental investigation on roughness element comprises of chamfered ribs with groove type roughness in order to get the improvement in heat transfer for the geometrical parameters taken into consideration. Kumar *et al.*[9] analyse the effect of heat transfer and friction factor phenomenon for twisted ribs roughened surface through the concept of LCT technique. Kumar and Layek[10] did an experimental work on the roughened surface of a solar air heater in order to get the optimal condition of Nusselt number and friction factor using the LCT technique. Kumar and Layek[11,12] observed through

his experimental analysis are that the solar air heater having winglet type roughness on the absorber plate achieve its highest value of heat transfer at P_i/e of 8, α of 60° and W/*w* of 5 through the concept of LCT technique. The highest enhancement value for Nusselt number and friction factor are recorded to be 2.95 and 2.84 times the smooth channel.

The present investigation deals to analyses the flow visualization for the roughened plate on the basis of surface temperature and the desired effect on heat transfer distribution over the surface, which is carried out with a different set of geometrical parameters considered. The non-dimensional parameters to define the roughness are relative roughness pitch (P_i/e), attack angle (α), relative roughness width (W/*w*) and the flow Reynolds number ranges from 13500–20500.

Experimental procedure

Rib geometry:

For a specific roughness element, the geometry and its shape is considered to be an important factor to achieve its target value on the basis of its operating conditions. Fig. 1 depict the schematic sketch diagram of the required winglet ribs used on the absorber surface for the investigation. The positioning and general geometry of the delta winglet type as a rib roughness on the absorber surface are depicted in Fig. 2. The non-dimensional parameters are considered and operating range are presented in Table 1. where 'e' nomenclature as the rib height.

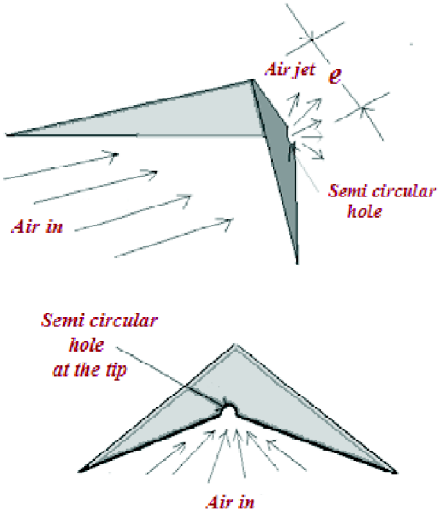

Fig. 1. Schematic sketch diagram of winglet rib.

Table 1. Operating parameters

Parameters	Ranges			
Relative roughness pitch (P_i/e)	6	8	10	12
Attack angle (α)	30°	45°	60°	75°
Relative roughness width (W/*w*)	3	4	5	6

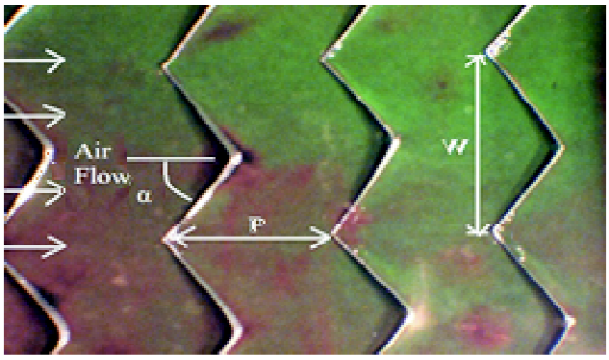

Fig. 2. Delta winglet ribs.

Experimental setup details

Fig. 3 represents the schematic sketch diagram of the experimental setup as well as the required instruments utilized in the solar air heater. The experimental setup consists a rectangular channel comprises of three sectional part namely inlet part, test part and exit part which is designed according to ASHARE Standard[13]. In addition to this, the illuminating system, CCD camera and a data logger along with a computer are also used. The experimentation is done in an open-loop flowing system and the length of the inlet and exit part as per the ASHRAE standard[13] is $5\sqrt{WH}$ and $2.5\sqrt{WH}$. Aluminum plate having a thickness of 3 mm act as a heat transfer surface placed inside the test section with an electric heater to provide uniform heat flux. The radiation

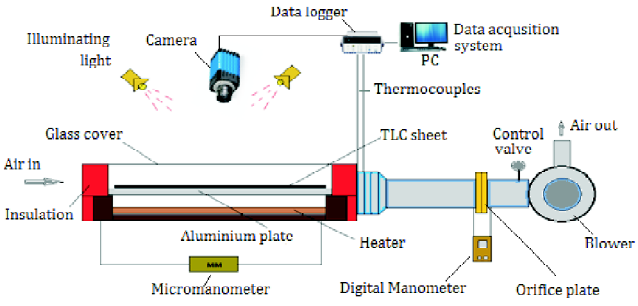

Fig. 3. Schematic diagram of an experimental set up.

effect is only considered for heating the absorber surface and the uniform amount of heat flux given to the absorber surface is absorbed by the radiation process only. T-type thermocouple (24 SWG) are used to record the air temperature for the inlet and exit section. A digital type micro-manometer is installed in a line to measure the pressure drop across the test section. An orifice meter along with a digital differential pressure gauge used to measure the velocity of the flowing fluid or mass flow rate. The photographic image of the experimental setup with its instrumental parts are depicted in Fig. 4.

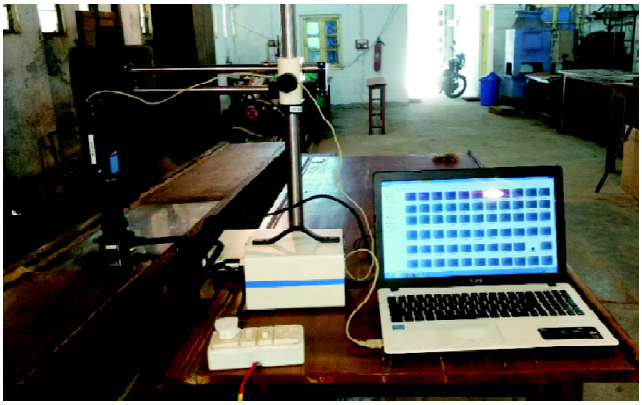

Fig. 4. Pictorial view showing experimental set up.

Image acquisition approach

The perception of the color distribution from the heated surface is captured by a 3CCD Sony camera connected to a computer to perceive the image from TLC (thermo chromic liquid crystal) sheet. An illumination source having 4 white light bulbs (each of 35 W power) has been used over the test zone. IC capture 2.3 software is used for capturing images in jpeg format. The activation of the color through TLC sheet visible only through in which the reflected light enters the CCD camera having a wavelength which splits into three beams and these beams accompanying red, green and blue arrays.

Image processing

The images which are captured by a camera are digitized in order to obtain its Hue, Saturation and Intensity (HSI) values from the red, green and blue ($R_rG_gB_b$) domain Kakade *et al.*[14] by eqs. (1)–(3). As Hue varies widely with the change in temperature compared to other parameters, therefore the variation in Hue is directly related to the surface temperature.

$$R_r = \text{Max; } H = \frac{G_g - B_b}{6\left(R_f - \min\left\{R_r, G_g, B_b\right\}\right)} \quad (1)$$

$$G_g = \text{Max; } H = \frac{2 + B_b - R_r}{6\left(G_g - \min\left\{R_r, G_g, B_b\right\}\right)} \quad (2)$$

$$B_b = \text{Max; } H = \frac{4 + R_r - G_g}{6\left(G_g - \min\left\{R_r, G_g, B_b\right\}\right)} \quad (3)$$

The saturation (S) values evaluated by

$$S = 1 - \left[\frac{\text{Min}(R_r, G_g, B_b)}{I}\right] \quad (4)$$

The required intensity (I) at a particular point obtained by,

$$I = \frac{R_r + G_g + B_b}{3} \quad (5)$$

Calibration curve for TLC sheet

The calibration of a TLC (thermo chromic liquid crystal) sheet consists of a heated plate where calibration has been done, controllable power supply and an image capturing system. A pre-packaged (R40C5W) TLC sheet is used for the visualization of temperature on the organic crystal materials which is used to get the color response in a reversible and repeatable pattern as the temperature changes. During the calibration process proper care and attention was taken in order to prevent interference from the surroundings light noise. The colorless image i.e. black color appears till it reaches the active temperature, it turns red, green and blue sequentially again turns to colorless when the temperature exceeds its active ranges. The color-temperature play interval depends on the TLC composition Stasieka *et al.*[15].

The calibration curve plotted for the hue-temperature relationship is shown in Fig. 5 and the relation obtained between temperature and hue is given by eq. (6)

$$T = -15.951\,H^4 + 57.538\,H^3 - 47.775\,H^2 + 39.391\,H + 310.52 \quad (6)$$

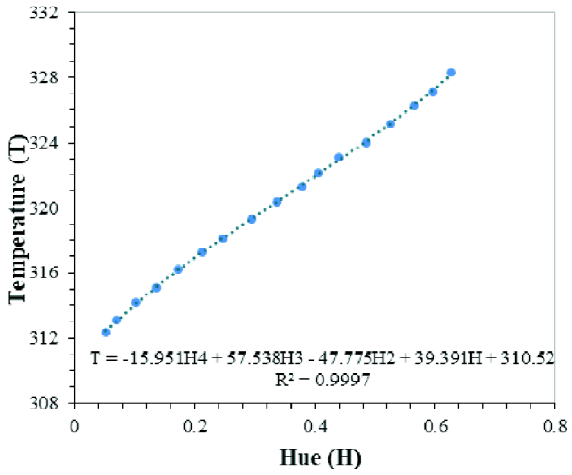

Fig. 5. Calibration curve for TLC sheet.

Data reduction

As the surface of the plate reached to steady state condition, the recorded TLC image which captured through a CCD camera are transformed it into a bmp files using frame grabber. The $R_rG_gB_b$ value of the sample images changes to that with HSI values only through pixel by pixel using the MATLAB software code. The TLC image obtained has been digitized to its hue values and these hue value thus used to calculate wall temperature to calculate convective heat transfer coefficient (h) given by using following relationship.

$$h = \frac{Q}{(T_{LCT} - T_{fm})} \quad (7)$$

where, Q noted as convective heat flux, T_{LCT} given in eq. (7) known to be heated plate temperature through the color output of the TLC sheet and T_{fm} is mean fluid temperature for the given x-position. For the given x-distance the following relation has been used to measure the mean fluid temperature of the flowing fluid.

$$T_{fm} = T_i + \frac{Q_{conv} A_p (x/L)}{mC_p} \quad (8)$$

The required value of Nusselt number (Nu) and Reynolds number (Re) thus used are given by using following relationship.

$$Nu = \frac{hDh}{k} \quad (9)$$

$$Re = \frac{VD_h}{\upsilon} \quad (10)$$

Fig. 6. depicts the LCT captured image over the smooth plate showing its $R_rG_gB_b$ (red, green and blue) values. In order to get the accuracy of the measurement the set up validation has been conducted for a smooth channel to obtain Nusselt number (Nu) as shown in Fig. 7 and the data which is obtained from the experimentation is used for the comparison with Dittus-Boelter Equation McAdams[16] given by eq. (11).

Dittus-Boelter equation:

$$Nu_s = 0.023Re^{0.8} Pr^{0.4} \quad (11)$$

The Nusselt number (Nu_s) deviation with the empirical relation for the smooth surface under fully developed flows condition deviated by 2.76%.

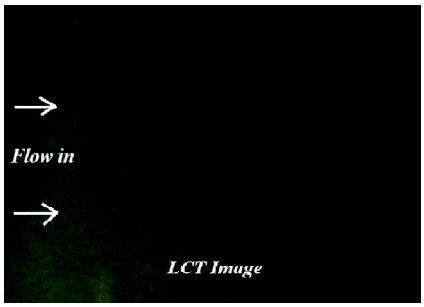

Fig. 6. LCT captured image over the smooth plate showing its $R_rG_gB_b$ (red, green and blue) values.

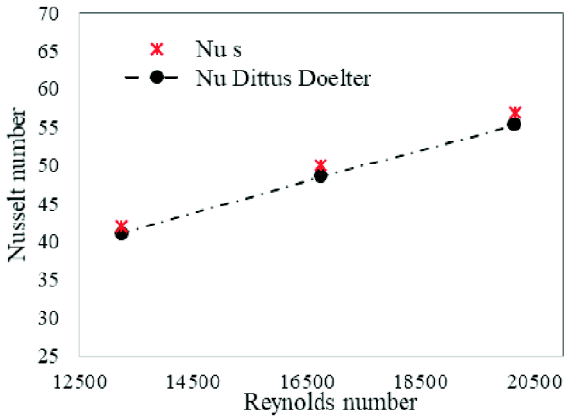

Fig. 7. Nusselt number vs Reynolds number for the smooth surface.

Experimental uncertainty

The error encountered mainly due to some experimental

uncertainty in the observed data which is suggested by Coleman and Steele[17]. The required uncertainty value recorded for (Nu) and (Re) at the 95% confidence level is noted to be of 3.69 and 3.82% respectively for Re=13500 and similarly, those for Re=20500 are 4.21 and 2.92% respectively.

Results and discussion

Effect of relative roughness pitch:

As depicted in Fig. 8, the roughness element was embedded on the heated side of the test surface in order to visualize the characteristics of temperature distribution using the liquid crystal optical system for the geometric arrangements at an angle of attack 60°, relative roughness width of 5 and varying relative roughness pitch of 6, 8, 10 and 12. The image thus obtained through LCT sheet has been used to get the local value of heat trantsfer coefficient.

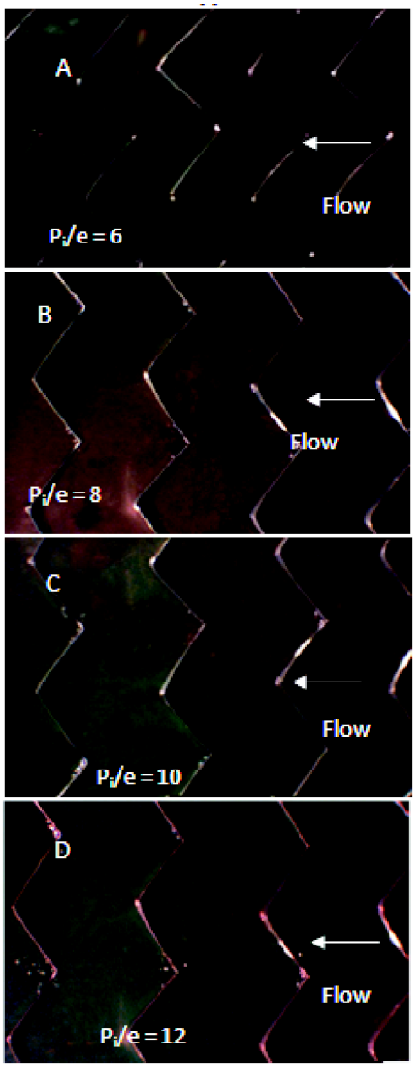

Fig. 8. LCT captured image at Re 20500 for P_i/e = 6, 8, 10, 12.

For relative roughness pitch of 6, flow reattachment at the consecutive ribs does not takes place in the inter-rib region as seen from Fig. 8 appears to be of green color due to its higher plate temperature. Further, increasing the P_i/e values to 8, red color appears between the inter-ribs and that region shows that the reattachment is possible. Further increase of P_i/e value to 10–12, the color response that appears gradually decreases and increases to the high intensity of green color, which clearly indicates that the flow reattachment between the ribs is supposed to be less than the previous arrangement. As presented in Fig. 9, it clearly shows that the Nusselt number is found to be less at P_i/e of 6, and attain its maximum values at P_i/e of 8 for all values of Reynolds number.

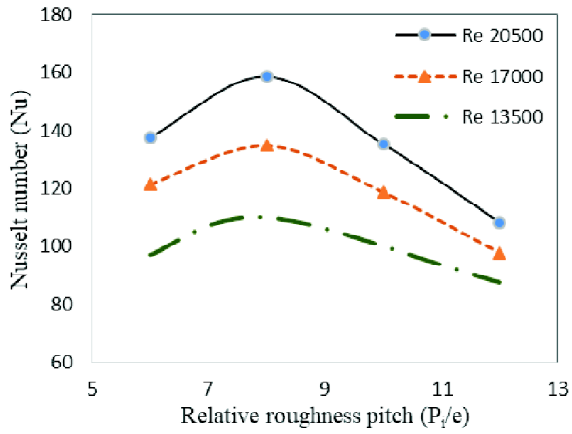

Fig. 9. Effect of relative roughness pitch.

The approximate flow pattern using a thin winglet type turbulator geometry with a small hole at the tip of the ribs produces formation of air-jet underside of the absorber surface as depicted in Fig. 10(a) and (b) could definitely prevent the formation of wakes just beside the ribs in the flowing stream and also creates the redevelopment of secondary flow through the leading ends of the ribs. In the present case, provision of the winglet shaped rib on the absorber surface is advantageous in many aspects as it reduces the thermal resistance generated by the presence of viscous sub layer just adjacent to the heated wall which minimises the eddies

or wake formation towards the flowing stream and behind the ribs.

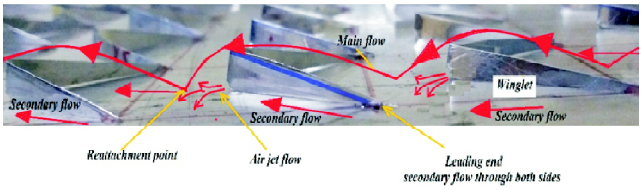

(a)

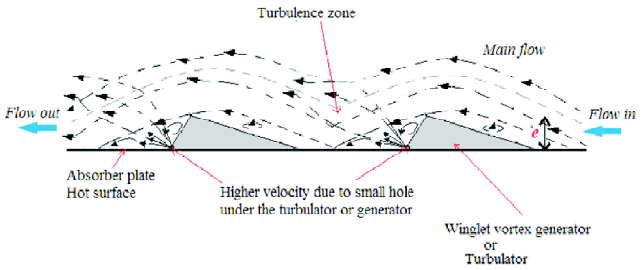

(b)

Fig. 10. (a) and (b) Pictorial and sketch view showing flow pattern anticipation.

Effect of attack angle

The winglet is arranged on the basis of angle of attack of 30°, 45°, 60°, and 75° as shown in Fig. 11, having a constant value of P_i/e of 8 and W/*w* of 5 to observe the temperature distribution in between inter-rib region. It can be seen from the Fig. 11 that for attack angle of 30°, 45° and 75° arrangement inter-rib space consists of green color respectively resulting higher value of plate temperature. At 60° angle of attack temperature distribution is shown (Fig. 11G), appears high intensity of red color mainly due to flow reattachment found to be high. The effect of attack angle on Nusselt number is depicted in Fig. 12, it is observed that the maximum Nusselt number attains at angle of attack of 60°.

Effect of relative roughness width

Fig. 13, shows the temperature distribution based on LCT study for the surface arrangements of α = 60°, P_i/e = 8 and at varying relative roughness width of 3, 4, 5 and 6. It can be seen from Fig. 13, K for W/*w* of 5, the high intensity of red color appears on the surface, mainly due to flow reattachment at different location supposed to be high. For arrangement of W/*w* of 3, 4 and 6, such images (Fig. 13I, J and L)

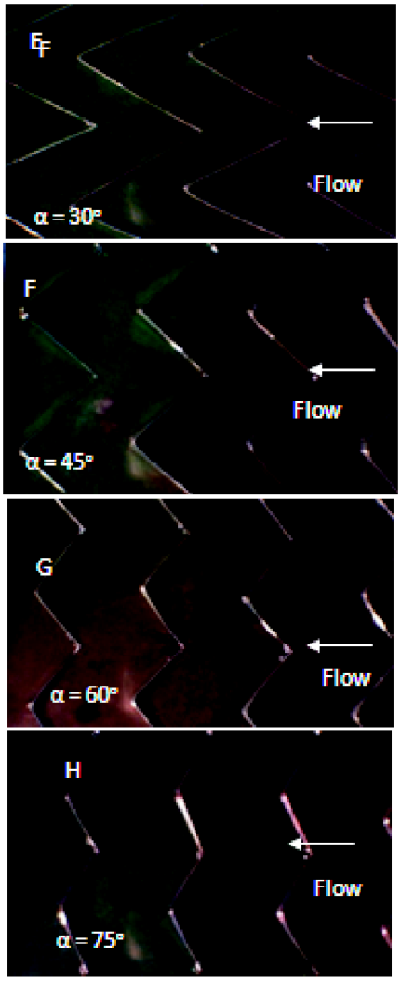

Fig. 11. LCT images captured at Re 20500 for angle of attack (α) of 30°, 45°, 60°, 75°.

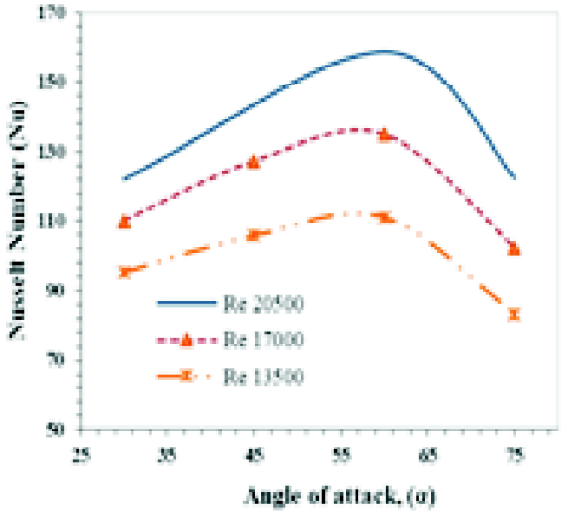

Fig. 12. Effect of attack angle (α).

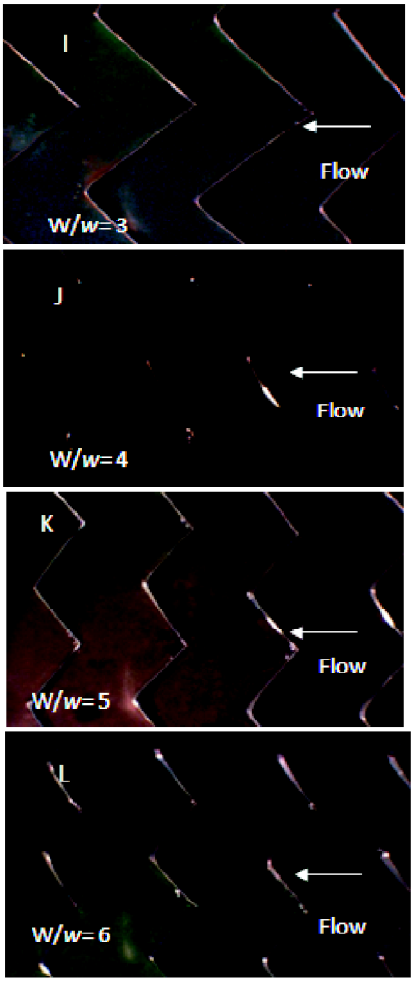

Fig. 13. LCT images captured at Re 20500 for relative roughness width of 3, 4, 5, 6.

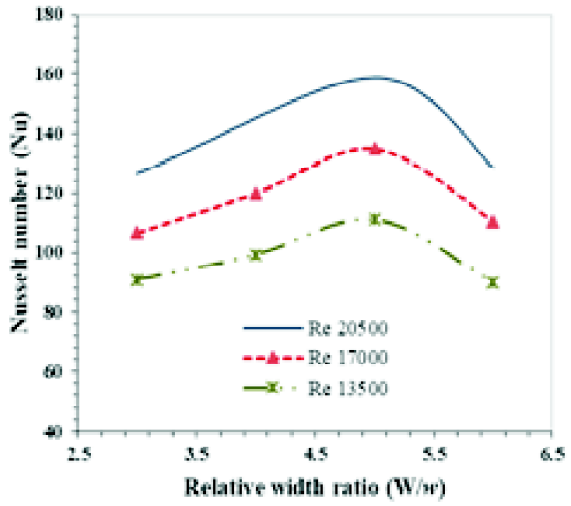

Fig. 14. Effect of relative roughness width (W/*w*).

appears high intensity of green color, indicates that the flow reattachment does occur properly of the free shear layer. Fig. 14, shows the effect of relative roughness width on Nusselt number, it can be observed that at W/*w* of 3 the Nusselt number is low leads to an optimum value of Nusselt number at W/*w* of 5 for all the values of Reynolds number and again decreases for further increase in W/*w* values.

Conclusions

The results showed that the application of LCT technique can provide the temperature distribution over a surface and are utilized to evaluate the local heat transfer coefficient in order to get further information about the flow field. The zone of reattachment point, vortex generated can be observed over a surface based on the application of LCT technique. A systematic study has been made for different configurations of winglet type rib geometries for evaluating the heat transfer distribution over the heated surface. Based on the present investigation the optimum values of heat transfer coefficient is seen at P_i/e of 8, W/*w* of 5 and α of 60°. Thus, the heat transfer measurement on the basis of its temperature distribution are strongly recommended to understand the detailed information regarding flow visualization.

Acknowledgements

The research work was funded by the SERB, DST, Govt. of India, Ref no.: SB/EMEQ 314/2013; dated: 08/07/2013.

Nomenclature

Ap	Absorber surface area (m^2)
Cp	Specific heat (air) (J/kg K)
h	Heat transfer coefficient (W/m^2K)
L	Length of absorber plate (m)
T_{LCT}	TLC sheet temperature (K)
T_{fm}	Mean fluid temperature (K)
Q	Heat flux (watt)
Nu	Nusselt number
k	Air thermal conductivity (W/mK)
m	Mass flow rate (kg/s)
V	Wind velocity of air (m/s)
Re	Reynolds number
υ	kinematic viscosity (m^2/s)
T	Temperature (°C)
H	Hue
D_h	Hydraulic diameter (m)

$R_rG_gB_b$	Red, green and blue
W/*w*	Relative roughness width
P_i/e	Relative roughness pitch

Greek symbol

α	Angle of attack
υ	Air kinematic viscosity
μ	Fluid dynamic viscosity
ρ	Air density

Subscript

r	Roughened surface
s	Smooth surface

References

1. T. L. Chan, K. Jambunathan and T. P. Leung, "A surface temperature calibration method for thermo chromic liquid crystals using true-colour image processing", Proceedings of the 10th International Heat Transfer Conference, Brighton, UK, 14-18 August 1994, Vol. 2, pp. 201.
2. T. E. Copper, R. J. Filed and J. F. Meyer, "Liquid crystal thermography and its application to the study of convective heat transfer, transactions of the ASME", 1975, 442.
3. A. Tariq, P. K. Panigrahi and K. Muralidhar, *Experiments in Fluids (Germany),* 2004, **37**, 701.
4. T. M. Liou, C. C. Chen and T. W. Tsai, *Journal of Heat Transfer*, 2000, **122**, 327.
5. G. Tanda, *International Journal Heat and Mass Transfer*, 2001, **44**, 3529.
6. D. Cavallero and G. Tanda, *Experimental Thermal and Fluid Science*, 2002, **26**, 115.
7. A. Tariq, S. K. Swain and P. K. Panigrahi, *Indian Journal of Engineering and Material Science,* 2002, **9**, 464.
8. A. Layek, J. S. Saini and S. C. Solanki, *Renew. Energy*, 2009, **34**, 1292.
9. A. Kumar and A. Layek, *Experimental Thermal and Fluid Science*, 2018, **97**, 205.
10. A. Kumar and A. Layek, *Thermal Science and Engineering Progress*, 2019, **14**, 100398.
11. A. Kumar and A. Layek, *Solar Energy*, 2020, **205**, 334.
12. A. Kumar and A. Layek, *Experimental Thermal and Fluid Science*, 2020, **23**, 110204.
13. ASHRAE Standards (93-77) Methods of testing to determine the thermal performance of solar collectors, New York.
14. V. U. Kakade, G. D. Lock, M. Wilson, J. M. Owen and J. E. Mayhew, *International Journal of Heat and Fluid Flow,* 2009, **30**, 939.
15. J. Stasieka, A. Stasieka, M. Jewartowskia and M. W. Collins, *Optics & Laser Technology*, 2006, **38**, 243.
16. W. H. McAdams, "Heat Transmission", Mc Graw-Hill, New York, 1942.
17. H. W. Coleman and W. G. Steele, "Experimentation and Uncertainty Analysis for Engineers", 2nd ed., John Wiley & Sons, New York, 1999.